LOAD ALLEVIATION AND RIDE SMOOTHING INVESTIGATIONS USING ATTAS

R. König, K.-U. Hahn
Institut für Flugmechanik
DLR-Braunschweig, FRG

Abstract

Aircraft employing modern wings with high aerodynamic efficiency and low wing loading are sensitive to gusts and turbulence and thus offer only limited passenger comfort in rough weather. Therefore, one important task of advanced active control systems is the reduction of effects of atmospheric disturbances acting upon the aircraft. This applies for the passenger comfort as well as for structural loads.

The Deutsche Forschungsanstalt für Luft- und Raumfahrt (DLR) has designed the Load Alleviation and Ride Smoothing System (LARS) to meet the above mentioned requirements. LARS has been implemented on the DLR Advanced Technologies Testing Aircraft System (ATTAS).

This paper represents the modelling of the ATTAS-aircraft, the design of the control system (open-loop rigid body control and closed-loop wing oscillation damping) and the results of simulations and first flight tests.

List of Symbols

a	acceleration
AC	aerodynamic centre
$\underline{\underline{A}}, \underline{\underline{B}}$,	matrices of a state space
$\underline{\underline{C}}, \underline{\underline{D}}$	quadruple
c.g.	centre of gravity
$C_{L\alpha WF}$	lift coefficient (wing, fuselage)
$C_{L\alpha HS}$	lift coefficient horizontal stabilizer
$C_{L\eta DLC}$	lift coefficient of the DLC-flaps
$C_{m\eta DLC}$	pitching moment coefficient of the DLC-flaps
DLC	direct lift control
EDP	electronic data processing
g	gravitational acceleration
H	height
K	gain coefficient
l_μ	mean aerodynamic chord
Mb	wing bending moment
n_x	longitudinal load factor
n_z	normal load factor
q	pitch rate
r_{HS}	distance between horizontal stabilizer and c.g.
r_S	distance between flight-log and c.g.
S	power density, wing reference area
S_{HS}	horizontal stabilizer reference area
T	time shift
T_{lag}	time lag
u	input
u_{Wg}	horizontal wind component
V	airspeed
w_{Wg}	vertical wind component
x	distance, state
x_N	distance between MAC of the wing and c.g.
y	output
α	angle of attack
α_E	horizontal stabilizer angle of attack
α_{HS}	angle of attack at the flight log
α_{dyn}	angle of attack addition caused by aircraft rotation
γ	flight-path angle
∂	denotes partial differentiation
Δ	difference
ϵ_{HS}	angle of the downwash
η	elevator deflection
η_{DLC}	DLC-flap deflection
θ	pitch attitude
λ	wavelength
λ_C	characteristic wavelength
σ	standard deviation
Φ	roll angle
ω	oscillation frequency
ω_c	corner frequency
Ω	spatial frequency

Subscripts

c	command
H	vertical acceleration
max	maximum
nz	load factor
seat	denotes a specific seat position
W	wind
$(\dot{})$	denotes time derivative
$(^*)$	denotes wing position
$(^{**})$	denotes elevator position
$(\_)$	denotes vector
1, 2..	index

I. Introduction

Wind disturbances, especially vertical gusts and vertical turbulence, create additional aerodynamic forces acting on wing, tail and fuselage to produce undesirable accelerations which greatly reduce passenger comfort. Furthermore, dynamic structural loads and gust strengths above the design limit can lead to permanent deformations of the structure or even crashes. A complete alleviation of gust effects requires aerodynamic counter forces at the same position, time and magnitude as the wind forces. This is in actuality impossible; gust alleviation systems can only reduce a part of the wind effects.

Structure loads, such as the wing bending moment, and the disagreeable vertical accelerations are produced principally by vertical winds. Horizontal turbulence or wind shear produce only small effects. Therefore this paper deals with vertical winds and their actuation upon the aircraft motion in the symmetrical vertical plane.

Effective gust alleviation can be obtained only if the wing has control surfaces for direct lift control, such as flaps at the trailing edge, symmetrical ailerons, or spoilers. Lift change by changing the angle of attack is generally not fast enough, because the aircraft must first rotate.

The two great problems of gust alleviation are the effectiveness and rates of the controls. Trailing edge flaps do not extend the full length of the wing and can therefore only compensate for the lift change due to a gust with a higher deflection, which in turn is less efficient and quietly leads to exceeded design limits. Furthermore, the deflection time increases with the greater amount of necessary deflection, so that the gust can pass by the wing by the time the aerodynamic counter force arises.

The objectives of gust/gust load alleviation systems are to increase the passenger ride comfort and the damping of structural modes, as well as to reduce peak loads, which can be produced by the 1-cos-design-gust. To meet these objectives, different approaches have been realized. Structural mode damping systems have been developed for the Lockheed 1011 [1], C-5A and Boeing B-52H. The ride-smoothing system OLGA [2] has been investigated by Dornier and DFVLR from 1976 to 1982. In recent years British Aerospace has demonstrated a gust load alleviation system to be used with the Airbus A320. This system has the objective of reducing peak loads.

II. Wind and Aircraft Modelling

For the design and development of a gust load alleviation system, modern digital computers combined with non-linear simulation techniques are quite helpful. To use these powerful tools, mathematical models of the lower atmospheric wind disturbances and the aircraft motion affected by wind are needed.

The most common gust model is a vertical wind with a 1-cos shape (see FIG. 1) [3]. This discrete gust is described by the maximum vertical wind $w_{Wg\ max}$ and the wavelength λ. Besides such deterministic gusts, a stochastic movement of the air can be observed in the atmospheric boundary layer. Mathematical models for formulating this phenomenon are available [4, 5]. The approach of DRYDEN is illustrated in FIG. 2. The power-spectrum shown represents the vertical wind distribution along the flight path.

The transformation of the time-dependent wind into an earth fixed wind-field can be made by using the TAYLOR hypothesis [6] whenever the aircraft airspeed V is much higher than the wind-speed V_W (see FIG. 3). The spatial wind frequency is then

$$\Omega = \omega / V \tag{1}$$

The power-spectrum of the wind-field can be calculated by

$$S(\Omega) = \frac{2\ \lambda_c\ \sigma_W^2}{1 + \lambda_c^2\ \Omega^2} \tag{2}$$

where σ_W is the standard deviation of the wind and λ_c is the characteristic wavelength. The latter represents the corner frequency and can be calculated by

(3) $$\lambda_c = 2 \pi V / \omega_c$$

Normally for the near-ground atmosphere λ_c = 150 m and σ_w = 1 m/s are good choices for a realistic standard situation [7].

The advantage of an earth-fixed windfield is a more realistic modelling of the wind distribution along the aircraft. However, a corresponding aircraft model is needed. The non-linear model used for the open-loop investigations is based on the motion of the rigid body aircraft with the wind acting on the plane calculated at three sections along the longitudinal axis (see FIG. 4). The wind in Section 1 is only important for the flight log sensor which measures the angle of attack, but the wind in Sections 2 and 3 directly affects the aircraft aerodynamics. The windfield is assumed to be time independent while the aircraft passes through at airpeed V.

The aircraft model shown in FIG. 4 represents a two-point aerodynamic model (wind considered at wing and horizontal stabilizer). The aerodynamic derivatives for such a model have been determined by the parameter identification method of the DLR [8]. FIG. 5 shows the efficiency of the DLC flaps. For the design of a gust alleviation system the actuator dynamics are as important as the aircraft dynamics. This is especially true for the actuators of the direct lift control flaps [2]. These actuators are identified and modelled with second-order dynamics with a deflection limitation of 35 deg and a maximum deflection rate of 75 deg/s. The time responses of the real and the modelled DLC-flaps are shown in FIG. 6. The elevator is represented with first order dynamics. Its maximum deflection rate is 30 deg/s.

Furthermore, all relevant components such as the electronic data processing system (EDP) are modelled, as are the sensor dynamics and time lags of the complete system. This extensive simulation of windfield, aircraft, sensors and EDP-system is used for the investigations into the open-loop portion of LARS and its design.

For the design of the closed-loop wing-oscillation damping and the calculation of the wing bending moment, an additional description of the elastic aircraft behaviour is needed. Finite element calculation methods along with structural excitation on the ground and during flight supply the necessary data to generate an elastic model [9]. FIG. 7 shows the first two elastic modes of ATTAS, the engine mode and the primary wing bending mode, which are considered in the analysis. Due to their high frequencies, modes beyond these cannot be influenced by the actuators. The two elastic resonant frequencies are 3.5 Hz (engine) and 5 Hz (first wing bending). Additional to the elastic modes, the instationary aerodynamic force of the DLC-flaps must be modelled. The linear differential equation system (state space system) used as the model has the following principle form:

$$\dot{\underline{x}} = \underline{\underline{A}}\,\underline{x} + \underline{\underline{B}}\,\underline{u}$$

$$\underline{y} = \underline{\underline{C}}\,\underline{x} + \underline{\underline{D}}\,\underline{u}$$

$$\underline{\underline{A}} = \begin{bmatrix} \text{Rigid} & \begin{matrix}\text{Rigid}\\ \hline \text{Elastic}\end{matrix} & & \\ \hline \begin{matrix}\text{Elastic}\\ \hline \text{Rigid}\end{matrix} & \text{Elastic} & & \\ \hline & & \text{Actuators} & \\ \hline & & & \begin{matrix}\text{Instat.}\\ \text{Aerody.}\end{matrix} \end{bmatrix}$$

Four rigid states, four elastic states, three actuator states and one state for the instationary aerodynamic amount altogether twelve states.

FIG. 8 shows a comparison of the wing tip vertical acceleration frequency response due to a DLC-flap input. Theoretical and flight test results differ by a small amount. The flight test results bases upon frequency sweep inputs of the DLC-flaps starting at 2 Hz and ending at 7 Hz.

III. LARS - Concept

The LARS-concept goals include the improvement of passenger comfort and the reduction of the wing bending moment. Therefore LARS consists of two subsystems (see FIG. 9).

For improving passenger comfort, an open-loop control system is used. It has the advantage of leaving the handling qualities of the aircraft unchanged, but it also requires a good knowledge of the aircraft parameters and a precise gust determination for the feed forward to the control surfaces. The open-loop part operates in the frequency range between 0.1 Hz and 1.0 Hz where passenger comfort is most affected by gusts and turbulence (see FIG. 10). The control activities of the DLC flaps excite the wing bending mode. For the damping of this motion, a closed-loop control system is chosen whereby the wing tip normal acceleration is fed back to the DLC flaps. To avoid coupling effects to the aircraft motion the acceleration signals are band-pass filtered. With respect to the wing oscillation frequency of about 5 Hz, this can only be done successfully with fast actuators and very small time lags.

III.1 Open-Loop Rigid Body Control

To maintain an undisturbed flight in gusty weather conditions, several actions have to be taken. Presuming that the wind angle of attack representing the wind disturbance

$$\alpha_W = - w_{Wg} / V \tag{4}$$

is known, the required control activities can be derived from the flight mechanics equations. At first the gust-induced lift has to be compensated by the DLC flaps mounted at the wing. Therefore the time shift between the measured wind disturbance at the flight log and its arrival at the wing, as illustrated by FIG. 4, has to be considered. The pitching moment belonging to the actual DLC flaps deflections are to be compensated with the elevator. When the changed downwash of the wing as well as the gust itself reaches the horizontal stabilizer, additional elevator deflections are required to avoid pitching moments.

The resulting feed forward gains depend only on the aerodynamic derivatives of the aircraft. Therefore the consideration of a linear function for the DLC flaps efficiency is sufficient, as previous investigations with linear, square and cubic attempts showed. With this the DLC flaps deflections are

$$\eta_{DLC} = \eta_{DLC}^{*} = \frac{C_{L\alpha WF} \dfrac{r_{HS} - x_N}{l_\mu}}{C_{L\eta DLC} \dfrac{r_{HS} - x_N}{l_\mu} C_{m\eta DLC}} (-\alpha_W^{*}) \tag{5}$$

where α_W^{*} is the wind angle of attack at the wing position. The elevator deflection is

$$\eta = \frac{\partial \eta}{\partial \alpha_{HS}} \Big[(1 - \partial \epsilon_{HS}/\partial \alpha) \quad (-\alpha_W^{**}) + (\partial \epsilon_{HS}/\partial \eta_{DLC}) \quad \eta_{DLC}^{**} + \frac{C_{L\alpha WF} \quad (x_N/l_\mu)}{C_{L\alpha HS} \quad (S_{HS}/S) \quad (r_{HS}/l_\mu)} \alpha_W^{*} + \frac{C_{L\eta DLC} \quad (x_N/l_\mu) + C_{m\eta DLC}}{C_{L\alpha HS} \quad (S_{HS}/S) \quad (r_{HS}/l_\mu)} \eta_{DLC}^{*} \Big] \tag{6}$$

where α_W^{**} is the wind angle of attack, η_{DLC}^{**} the DLC flaps deflection producing the induced downwash at the horizontal stabilizer position, and η_{DLC}^{*} the actual DLC flap position.

FIG. 11 gives the block diagram of the open-loop system. For a fixed aircraft configuration the control law can be reduced to a system with constant coefficients:

$$\eta_{DLC} = \eta_{DLC}^{*} = K1 \; (-\alpha_W^{*}) \tag{7}$$

$$\eta = K24 \; (-\alpha_W^{**}) + K21 \; \eta_{DLC}^{**} + K22 \; \alpha_W^{*} + K23 \; \eta_{DLC}^{*} \tag{8}$$

Thus, all the required control surface deflections can be derived from the wind angle of attack and the time shifts necessary for time coordinated actions. The time shift between the registration of the gust at the flight log position and the action of the DLC flap can be determined by (see FIG. 4)

$$T_1 = (r_S + x_N) / V \tag{9}$$

To cover the distance between the wing and the horizontal stabilizer, the wind disturbance and the changed downwash needs the time

(10) $T_2 = (r_{HS} - x_N) / V$

As Equations (9) and (10) suggest, the time shifts are not constant but rather airspeed dependent.

The theoretical time shifts above can be used for the compensation of system time lags of the sensors, EDP and actuators. The relevant total time shifts then become

(11) $T_{T1} = T_1 - T_{lag}$

(12) $T_{T2} = T_2 - T_{lag}$

as used in FIG. 11.

To insure that no unnecessary control activities occur at higher frequencies, the control signals are low-pass filtered. To achieve similar system dynamics for elevator and DLC flaps, the low-pass filter of the DLC signal has a higher time constant than the filter for the elevator signal. In this manner, the deflections of the two control surfaces fit together in magnitude and phase over the relevant frequency range.

III.2 Closed-Loop Wing Oscillation Damping

Most transport aircraft have only small damping of the first wing bending mode. Therefore, excitations with great dynamic loads are easily produced by turbulence or active control systems, such as the described open-loop gust alleviation system. A wing oscillation damping system may be necessary and so has been investigated for use with ATTAS.

FIG. 12 shows the block diagram of the designed closed-loop system. The vertical accelerations of the left and right wing tip are combined, reduced by the centre of gravity vertical acceleration, band-pass filtered and then fed back to the DLC-flaps. Due to the low characteristic frequency of the DLC actuator, acceleration instead of velocity is fed back to increase the damping of the wing bending mode. To determine the value of the gain K3, the root-locus method was used (FIG 13). A maximum damping coefficient is obtained with K3=-0.5. Except for the DLC-actuator, the other modes do not change.

The time response of the wing bending moment due to a vertical wind step is shown in FIG. 14. Compared with the uncontrolled system, the damping increases distinctly and the overshoot is reduced by about 35%. Time delays produced by the data processing will increase the damping when they are less than 20 ms (FIG. 15), but the system becomes instable should they be greater or equal to 30 ms. The sampling time of the digital data processing system of ATTAS amounts to 25 ms, which is already critical. Todate, the improvement of the damping of the wing bending mode has been investigated only using simulation methods. Flight test investigations are planned for the near future.

IV. Implementation on ATTAS

The efficiency of the open-loop passenger comfort improvement depends on the accuracy of the knowledge of the aerodynamic derivatives as well as the precise determination of the wind angle of attack. Therefore, the sensors available on board the aircraft are very important. In principle, α_W can be calculated by

(13) $\alpha_W = \alpha_L - \theta + \gamma + \alpha_{dyn}$

where α_L is the angle of attack measured by the flight log sensor, θ is the pitch attitude, γ is the flight path angle and α_{dyn} is an additional angle induced by the rotation of the aircraft. Normally the flight path angle signal produced, for example, by Inertial Navigation Systems is slow and extensively filtered and thus cannot be used for the LARS purposes. Neglecting horizontal wind effects and assuming small angles EQ. (13) can be written

(14) $\alpha_W = \alpha_L - \theta + \frac{\dot{H}}{V} + \frac{q\, r_S}{V}$

where $\dot{H}$ is the actual vertical speed of the aircraft and q is the pitch rate. The value r_S is the distance between the angle of attack sensor and the centre of gravity.

The block diagram of the wind angle of attack determination used in LARS is shown in FIG. 16. The vertical speed is calcu-

lated very precisely by a complementary filter [10]. At the position of the flight log the angle of attack α_L is mixed with the eigenmotion of the sensor, which itself has very low damping. After conditioning, the measured signal has to be NOTCH filtered to separate out this unwelcomed effect. At last the calculated wind angle of attack is sent through a high-pass filter to extract low wind frequencies which cannot be compensated with lift variation but rather with thrust variation [11]. Another advantage of the high-pass filter is the washing out of offsets of the wind angle of attack signal.

The complete open-loop control system as given by FIG. 11 and FIG. 16 is implemented in the ATTAS EDP system. It is programmed in FORTRAN which is easy to handle should program modifications be necessary. The user-software is connected to the ATTAS fly-by-wire/light capability by pre-defined data transfers using COMMON-block structures for the sensor inputs and the control outputs [12]. The frequency of a complete process cycle is 40 Hz. Therefore, the time delays calculated by EQs. (11) and (12) can be met within the sampling accuracy of 25 ms.

V. Simulation and Flight Test Results

The LARS open-loop controller to be implemented on ATTAS was designed with the help of the non-linear simulation (compare Chap. II) and the universal optimization procedure EXTREM [13]. Regarding the normal acceleration or respective load factor, the following design criterion was used

$$(15) \qquad n_{z\,seat} = n_z + (\dot{q}\ r_{seat}) / g$$

This is a joint criterion including translationary and rotationary aspects for a defined seat position, where r_{seat} is positive for seats in front of the centre of gravity. For the investigations and the optimization the pilot seat and the position of the last seat row in the aircraft tail were chosen. The results of the optimization show that the gain coefficients must be higher and the signal time shifts shorter than those predicted from the theory given by EQs. (7) and (8).

The vertical acceleration or the load factor of the centre of gravity is displayed in the following figures. A simulated flight through a 1-cos upwind gust is illustrated by FIG. 17. The efficiency of the LARS open-loop controller is obvious as can be gathered from the improvement of the load factor. The maximum load factor is reduced with LARS from $n_z = 1.18$ to $n_z = 1.04$ and the standard deviation is improved by $\Delta\sigma_{nz} = 75\%$ over the observed time period. Nearly the same is true for discrete gusts with other wind maxima. Also an other effect comes out by FIG. 17. Reducing the normal acceleration increases the longitudinal acceleration because this degree of freedom is not considered due to a shortage of adequate control surfaces. But from the theory of the conservation of energy, energy transfer from the normal to the longitudinal direction takes place by the factor g/V. Therefore the additional longitudinal accelerations resulting from the LARS activities are much smaller than the normal accelerations due to vertical turbulence without LARS.

The pitch reaction of the aircraft is only slightly improved. The investigations show that it is more efficient to accept a smooth aircraft rotation of the aircraft to maintain the angle of attack. This additional reduction of the wind angle of attack combined with a smaller lift variation gives better results than suppressing the rotation to reduce $\dot{q}$ and its effect on $n_{z\,seat}$ (compare EQ. (15)). This is even true for normal accelerations at positions far away from the centre of gravity.

In FIG. 18 the simulation results with LARS off/on of a flight in the DRYDEN wind-field are plotted. In general, the same statements are true as discussed before. The reduction of the normal acceleration can clearly be seen. The standard deviation of n_z is reduced by more than $\Delta\sigma_{nz} = 50$ %. FIG. 19 shows the power spectrum of the load factor with an improvement of more than 10 dB in the relevant frequency band. For lower frequencies around the phugoid, a deterioration occurs. This is because the LARS control activities stimulate the phugoid mode. But the aircraft response in this frequency band is easily controlled by a pilot or an autopilot.

The first flight test results with the open-loop controller show similar results (see FIG. 20 and FIG. 21). At the time this paper was written, only flight tests in weak turbulence were available. Thus the standard deviation of the vertical wind in FIG. 20 is only σ_W = 0.35 m/s. Although the wind disturbances are somewhat smaller for the LARS-on phase, the efficiency of the real system is obvious.

It is evident that the pilot has full authority for the aircraft, especially for flight path control. The feed-forward controller of LARS has no noticeable effect on the handling qualities. This becomes clearer in FIG. 22 where a flight in calm air with a computer generated elevator input is shown. The calculated wind angle of attack α_W during this manoeuvre as well as the resulting DLC-flap reactions are small. Therefore the effect on the handling qualities can be neglected.

VI. Conclusions

The load-alleviation and ride-smoothing system LARS has been designed using simulation and optimization techniques. Therefore complex mathematical models of atmosphere, rigid and elastic aircraft, actuators, sensors and data processing system have been developed. The LARS concept consists of a rigid body open-loop control system and an elastic mode closed-loop damping system. First flight test results of the rigid body controller already show the expected alleviation of vertical accelerations in turbulence. The damping of the first wing bending mode (closed-loop controller) can be significantly improved as simulation results illustrate. Flight tests of this LARS-component have yet to be performed.

The objective of the LARS-program is directed to the acquisition of knowledge about passenger comfort under consideration of structure load alleviation, effects on flight path accuracy and pilot workload reduction. Upon completion the implementation of the complete LARS on ATTAS, an excellent tool for this objective will be available.

References

[1] O'Connell, R.F.
Design, Development and Implementation of an Control System for Load Alleviation for a Commercial Transport Airplane.
AGARD Report No. 683,
Porz-Wahn, 1979.

[2] Böhret,H.; Krag,B.; Skudridakis,J.
OLGA - An Open-Loop Gust Alleviation System.
AGARD CP Nr. 384,
Toronto, Kanada, 1985.

[3] Background Information and User Guide for MIL-F-9490 D, Flight Control System-Design, Installation and Test of Piloted Aircraft.
Technical Report AFFDL-TR-74-116,
The Boeing Company,
Wichita Devision, Kansas, 1975.

[4] v. Kárman, TH.; Howarth, L.
On the Statistical Theory of Isotropic Turbulence.
Proc. Royal Society, A 164, 1938.

[5] Dryden, H.L.
A Review of Statistical Theory of Turbulence.
Quarterly Journal of Applied Mathematics 1, 7-42, 1943.

[6] Taylor, G. I
The Spectrum of Turbulence.
Proc. Royal Society, A 164, 1938.

[7] Schänzer, G.
Flug in gestörter Atmosphäre.
Vorlesungsmanuskript zur Vorlesung am Institut für Flugführung der TU Braunschweig, 1983.

[8] Rolf, D.; Mönnich, W.
ATTAS-Systemidentifizierung, Auswertung von Flugversuchen zum Leistungsnachweis des DLC-Klappensystems.
IB 111-87/3,
Institut für Flugmechanik,
DFVLR Braunschweig, 1987.

[9] Potthoff, U.
Ein mathematisches Modell des elastischen Flugzeugs mit instationärer Aerodynamik für flugmechanische Anwendungen.
IB 111-87/14,
Institut für Flugmechanik,
DFVLR Braunschweig, 1987.

[10] Redeker, A.; Vörsman, P.
Precise Vertical Speed Reconstruction Based on Vertical Acceleration and Barometric Altitude.
Z. Flugwiss. Weltraumforsch. 9,
Heft 4, Köln, 1985.

[11] Hahn, K.-U.
Effect of Wind Shear on Flight Safety. Prog. Aerospace Sci. Vol.26, Pergamon Press, Great Britain, 1989.

[12] Bauschat, J. M.
Der Experimental- und Regelrechner des Flugversuchsträgers ATTAS -Die Einbindung von Benutzer-Software- .
DLR-BR 111-13-89-010, Institut für Flugmechanik, DLR Braunschweig, 1989.

[13] Jacob, H.-G.
Rechnergestützte Optimierung statischer und dynamischer Systeme.
Fachberichte Messen-Steuern-Regeln, Hrsg.: M. Syrbe und M. Thoma, Springer Verlag, Berlin-Heidelberg-New York, 1982.

[14] Rohlf,D.; Schafranek,D.; Wilhelm,K.
Recent Results with ATTAS In-Flight Simulator.
AIAA Flight Simulation Technologies Conference, Atlanta, GA, 1988.

Figures

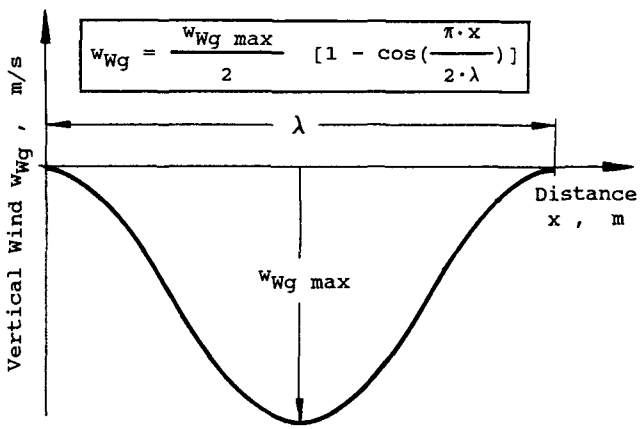

FIG.1 Shape of a (1-cos) Gust

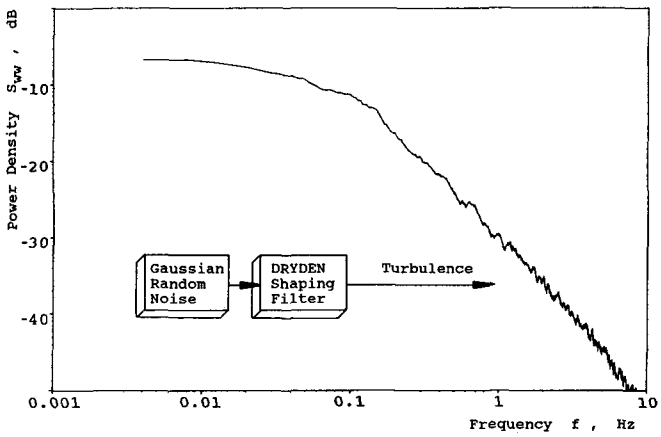

FIG.2 DRYDEN Pseudo Random Turbulence and Gusts

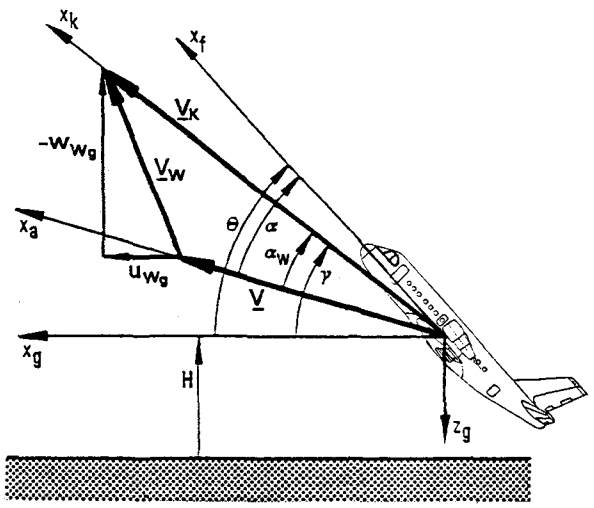

FIG.3 Vector Diagram of Speeds

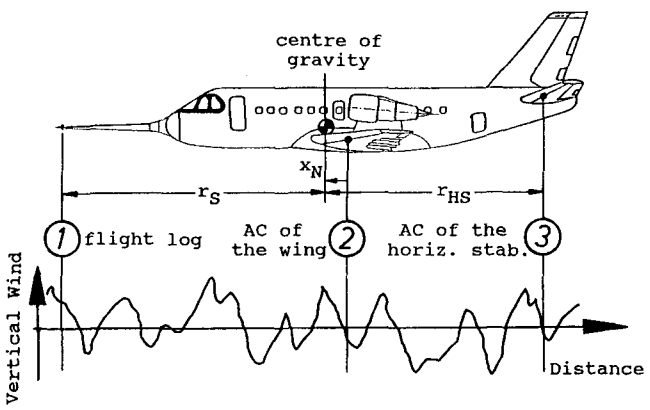

FIG.4 Multi-Point Rigid Body Aircraft Model

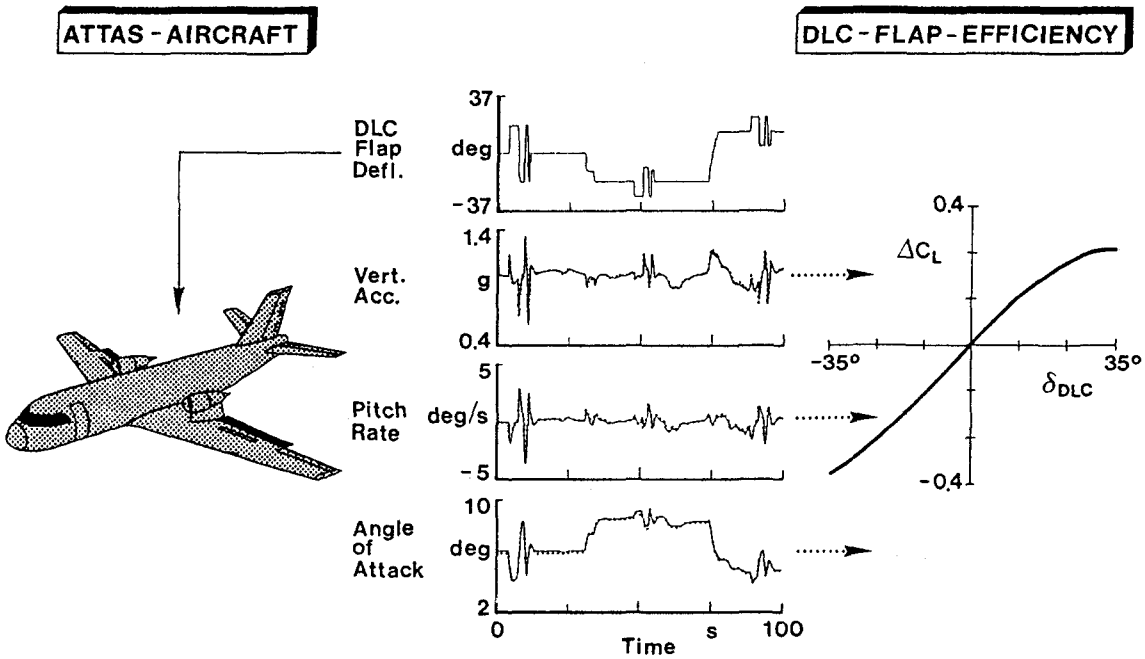

FIG.5 Identification of the DLC-Flap Efficiency [14]

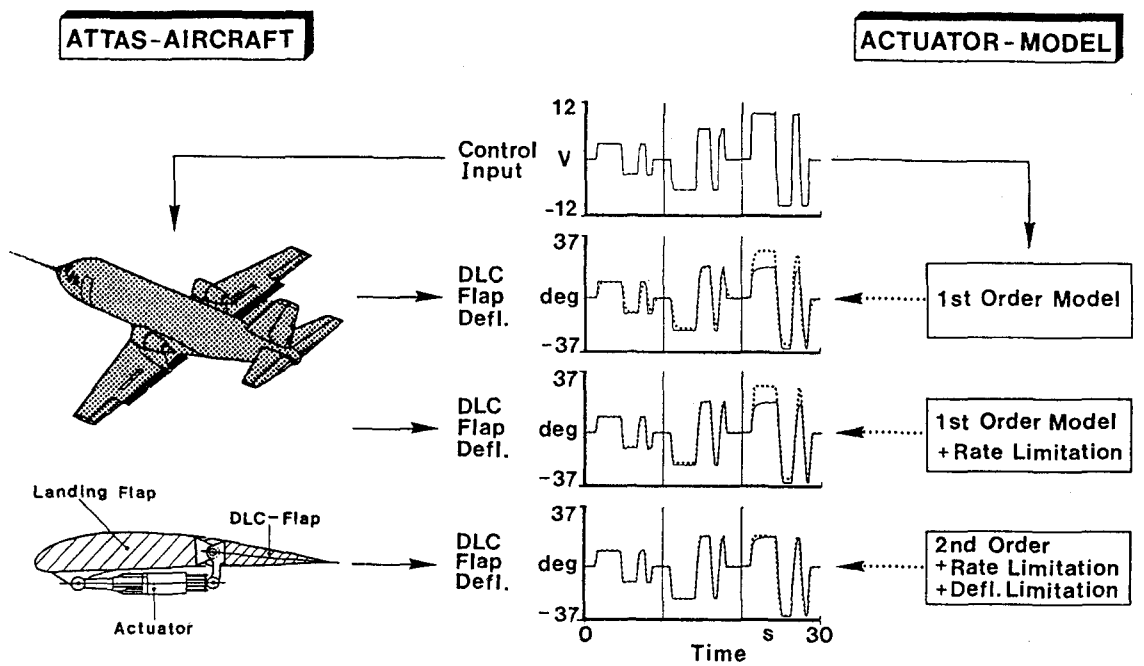

FIG.6 Identification of the DLC-Flap System [14]

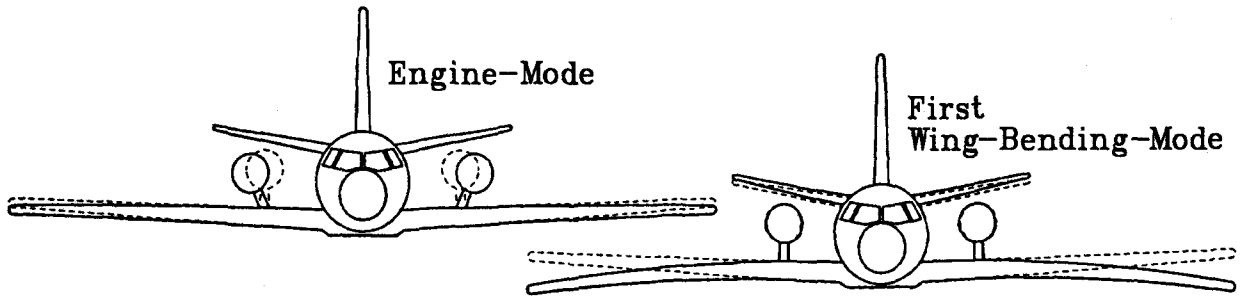

FIG.7 ATTAS Elastic Modes

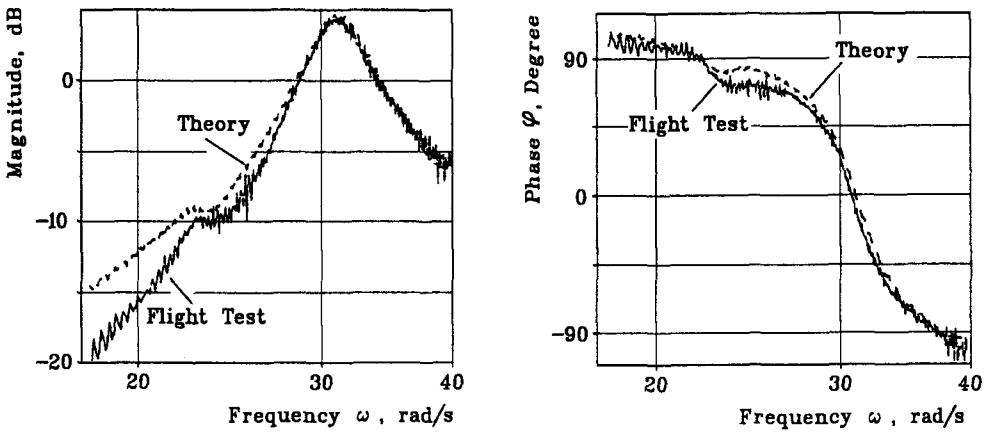

FIG.8 Comparison of Flight Tests and Theoretical Results

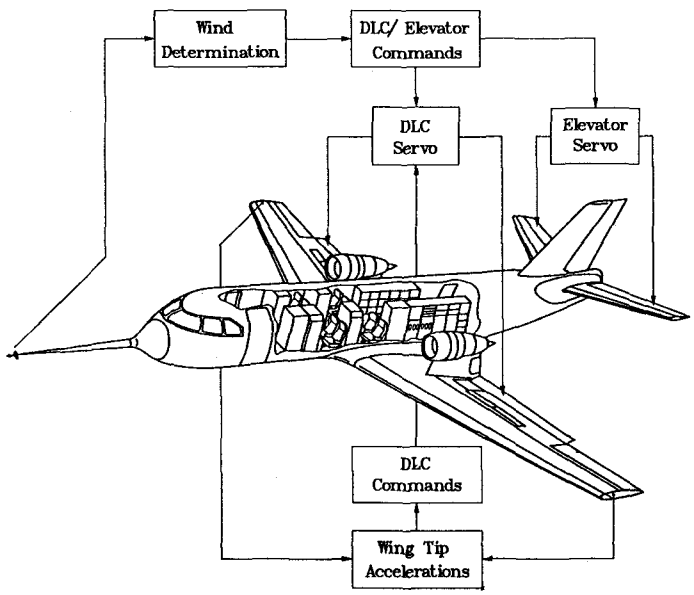

FIG.9 LARS Concept of Gust Load Alleviation

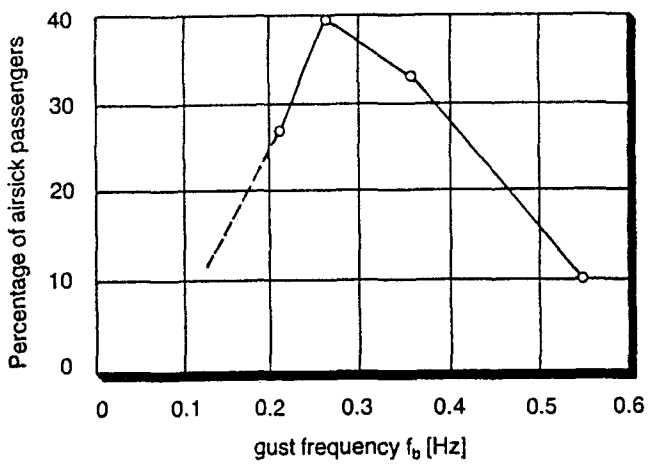

FIG.10 Percentage of Passengers to Get Airsick as a Function of the Gust Frequency [2]

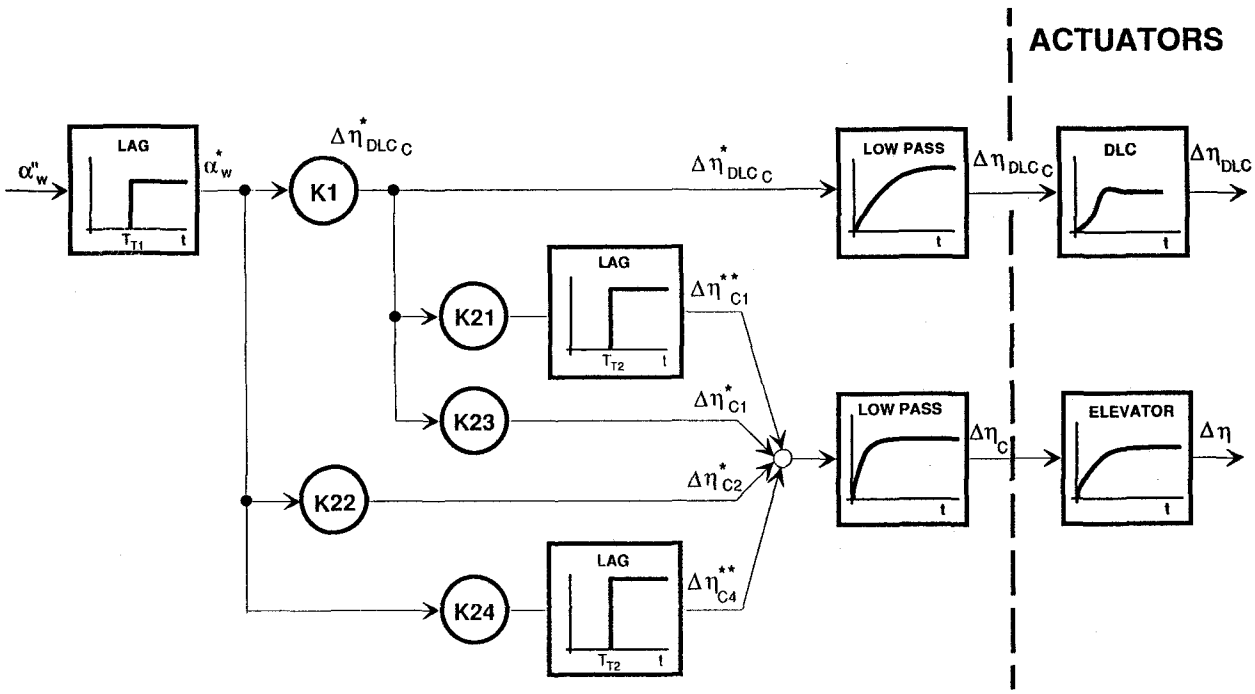

FIG.11 Block Diagram of the LARS Open-Loop Subsystem

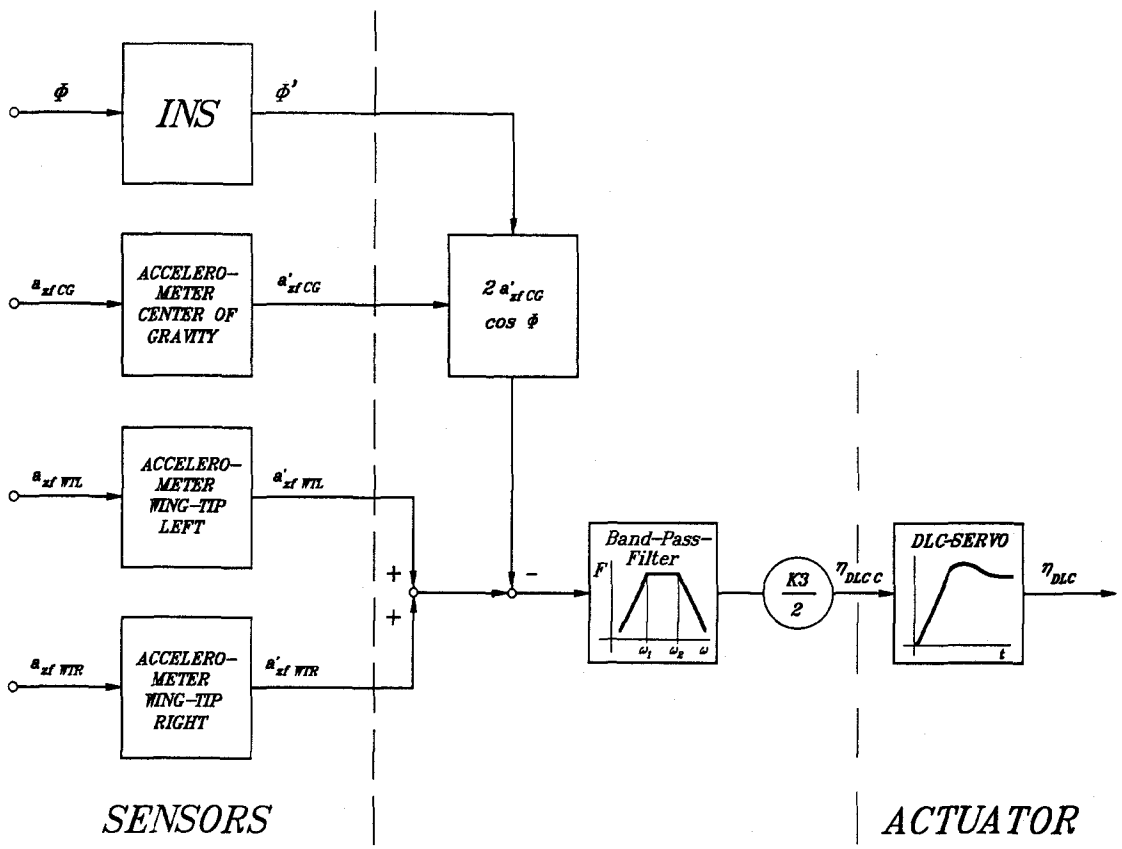

FIG.12 Block Diagram of Wing Oscillation Determination

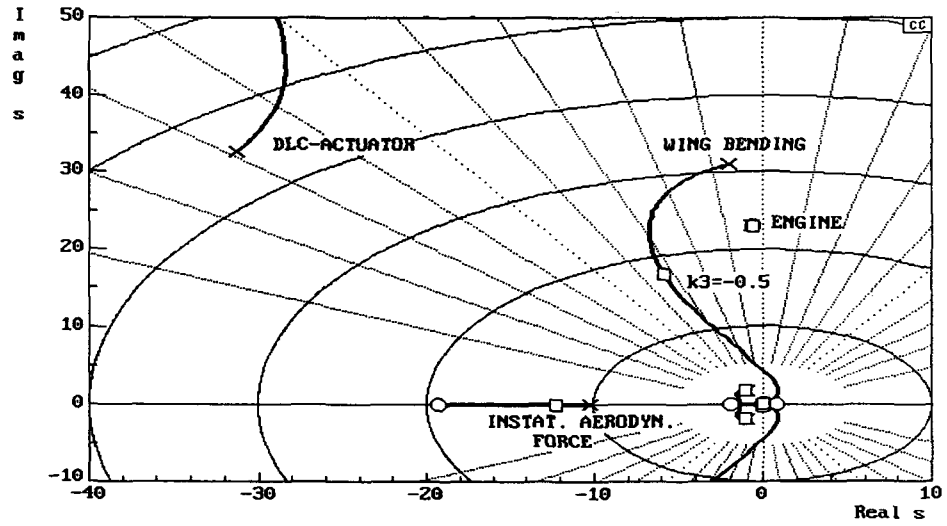

FIG.13 Root-Locus to Perform the Gain for the Wing Oscillation Damping

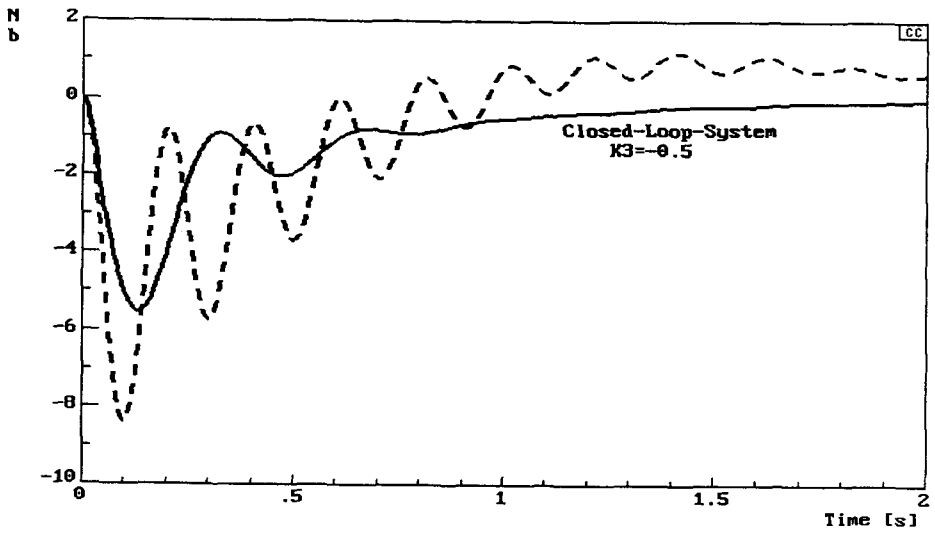

FIG.14 Time Response of Wing Bending Moment after a Step in Vertical Wind

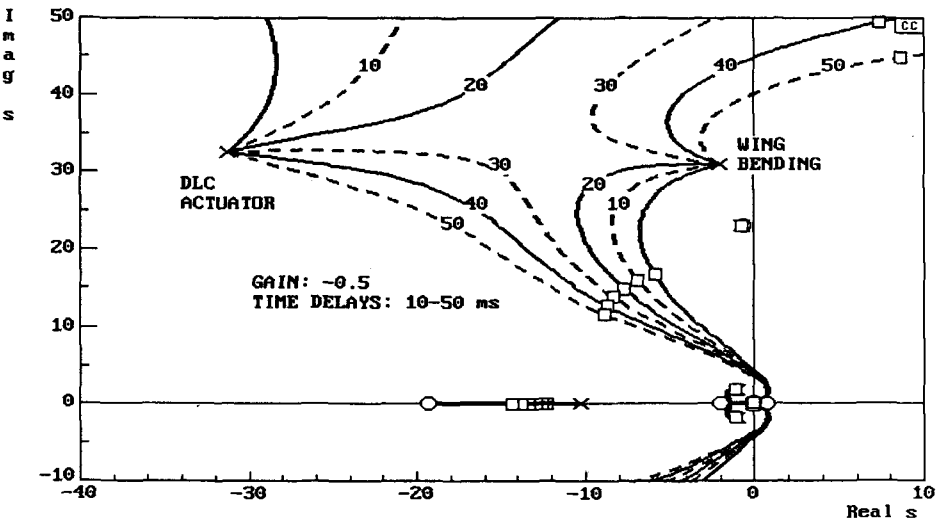

FIG.15 Influence of Time Delays for the Gain Design

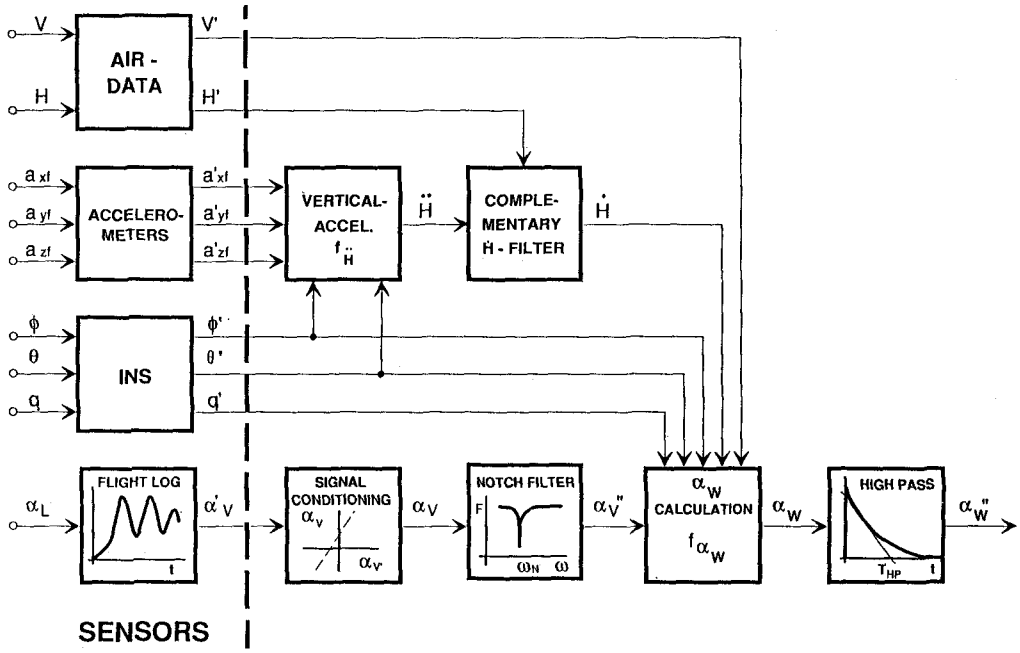

FIG.16 Block Diagram of the Wind Angle of Attack Determination

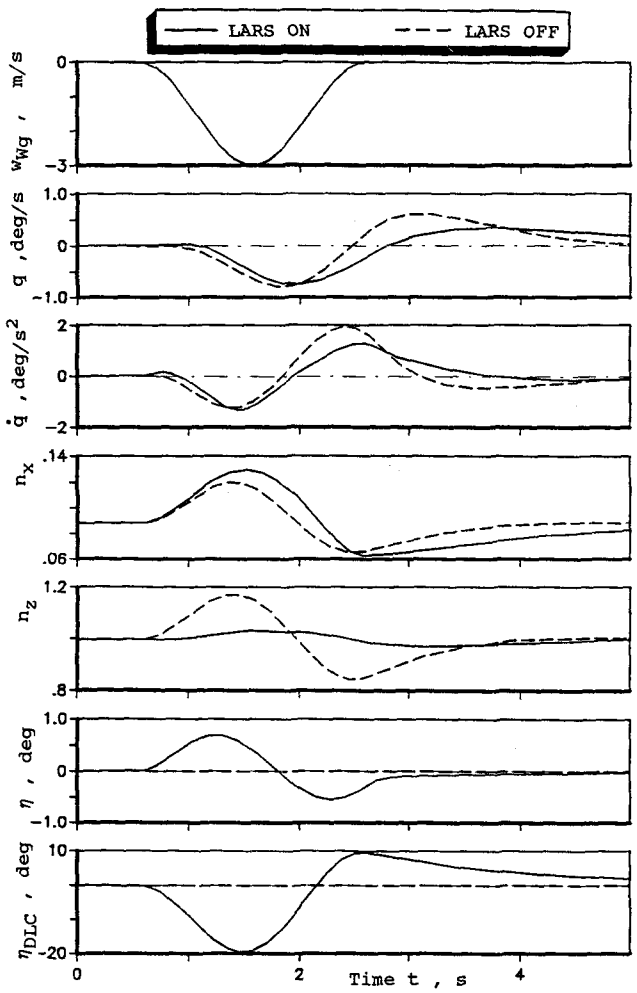

FIG.17 Flight Through a (1-cos) Gust (Simulation with: $w_{Wg\ max} = -3m/s$, $\lambda_c = 150m$)

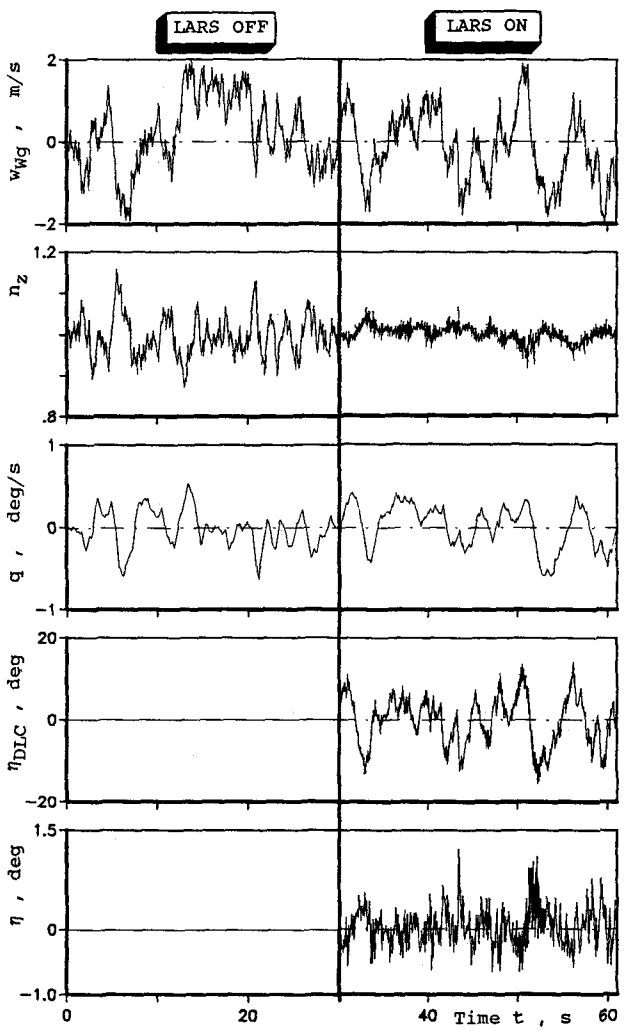

FIG.18 Flight in Turbulence (Simulation with $\sigma_w = 1m/s$)

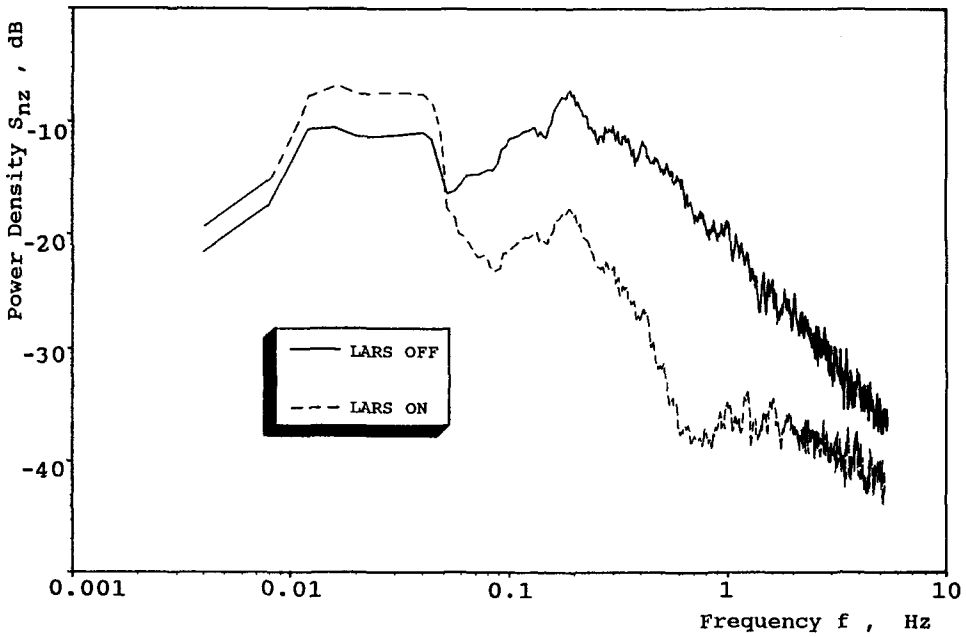

FIG.19 Power Spectrum of the Load Factor
(Simulation with σ_w = 1m/s)

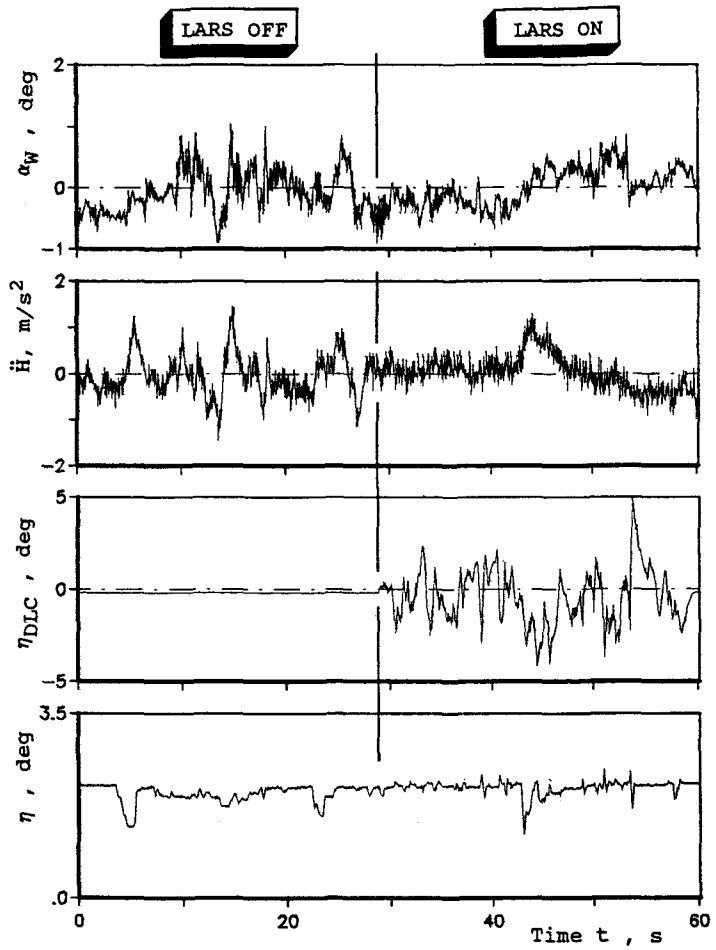

FIG.20 Flight in Atmospheric Turbulence
(Flight Test with σ_w = 0.35m/s)

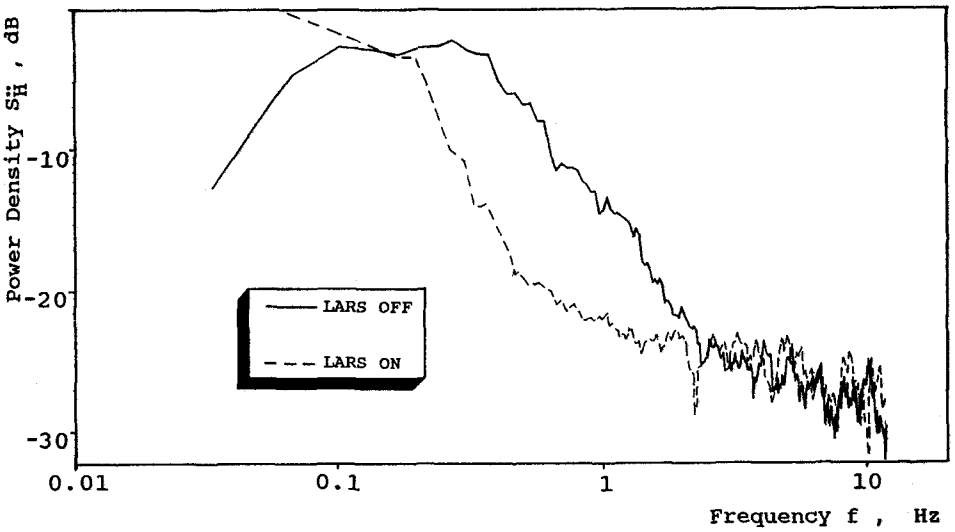

FIG.21 Power Spectrum of the Normal Acceleration (Flight Test with σ_w = 0.35m/s)

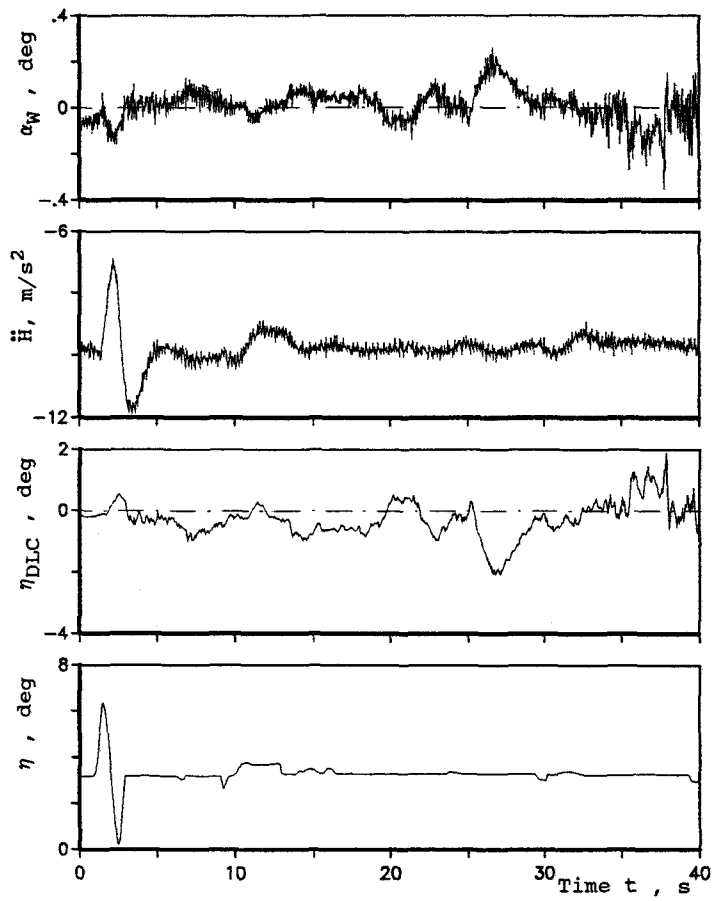

FIG.22 DLC-Flap Response to Elevator Control Inputs